Electronic Supplementary Material (ESI) for Soft Matter.

Supporting Information

Simulation and practice of particle inertial focusing in 3D-printed serpentine microfluidics via commercial 3D-printers

Pengju Yin,[a] Lei Zhao,[a] Zezhou Chen,[a] Zhiqiang Jiao,[a] Hongyan Shi,[a] Bo Hu,[*,a] Shifang Yuan,[*,b] Jie Tian,[*,a,c]

a School of Life Science and Technology, Library, Xidian University, Xi'an 710126, Shaanxi, People's Republic of China. Email: E-mail: bohu@xidian.edu.cn;

b Institute of Automation, Chinese Academy of Sciences, Beijing 100190, People's Republic of China. Email: jie.tian@ia.ac.cn;

c Department of Vascular and Endocrine Surgery, Xijing Hospital, The Fourth Military Medical University, Xi'an 710032, Shaanxi, People's Republic of China. Email: shifangy@fmmu.edu.cn;

* Correspondence: bohu@xidian.edu.cn; shifangy@fmmu.edu.cn; jie.tian@ia.ac.cn

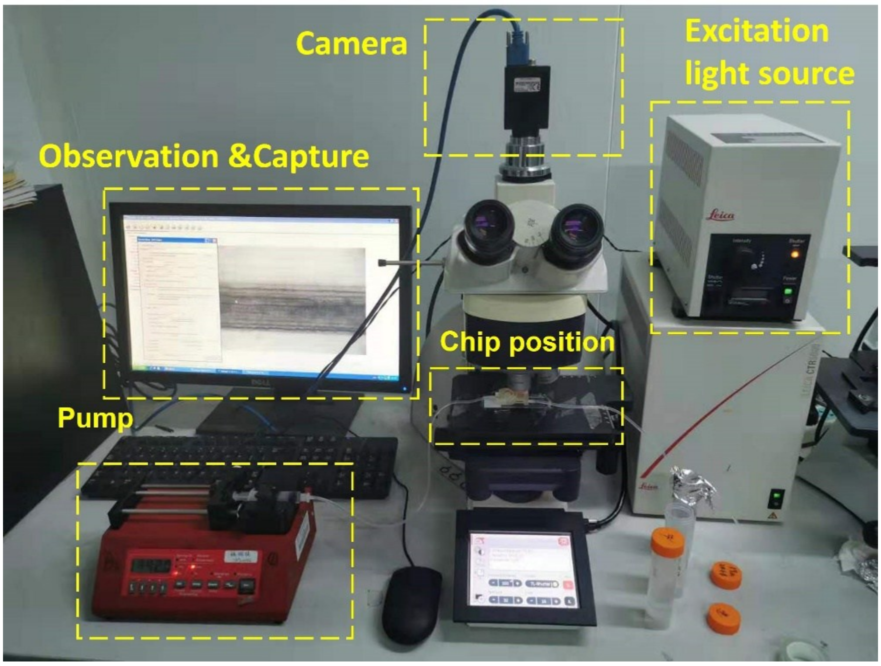

Fig. S1. Explanatory Chart of observation and capture images under particle focusing fluorescent experiment

Table S1. The technical details of Inkjet, SLA, DLP and FDM 3D printers.

Print function	Inkjet	SLA	DLP	FDM
3D-printer	Projet 3600HD	Form 1+	Miicraft +	Guiders
Build size	298X185X203mm	125X125X165mm	43X27X180mm	280X250X300mm
XY resolutions	25-50µm	155µm	56µm	100µm
Z resolutions	16µm	25-200µm	30-100µm	100µm
Print material	UV Curable Plastic	Photopolymer	Photopolymer, BV-003	ABS， PLA
Print head	Multi-nozzle	Single laser	Surface forming	Single nozzle
Print speed	Medium	Medium	Medium	High
Print cost	High	Medium	Medium	Low
Input Data File	STL, CTL, OBJ, PLY, ZPR, ZBD, AMF, WRL, 3DS, FBX, IGES, IGS, STEP, STP, MJPDDD	STL, OBJ	STL	3MF, STL, OBJ, FPP, BMP, PNG, JPG, JPEG

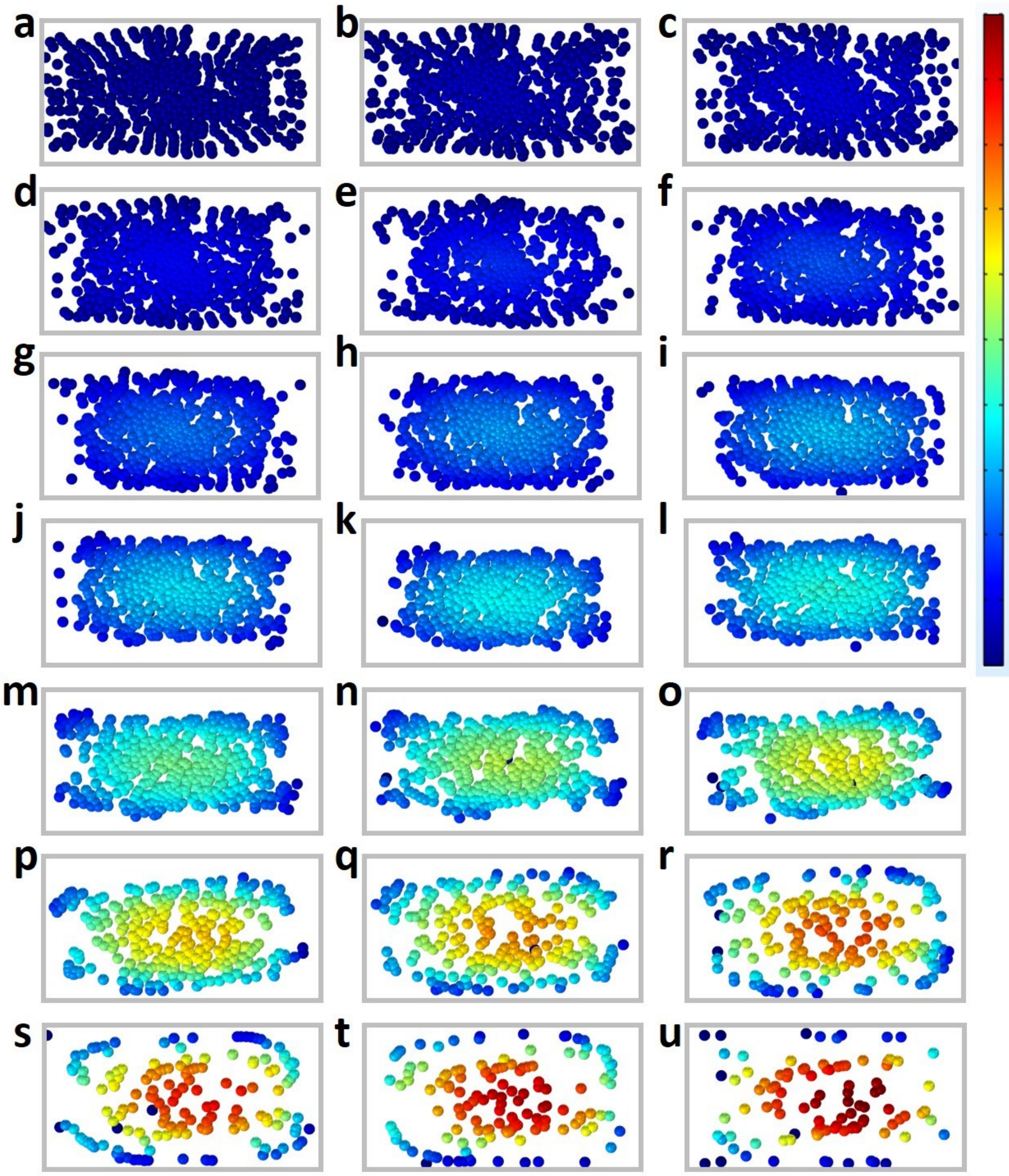

Fig. S2. The simulation results of different velocities (48 μL/min – 2832 μL/min) in serpentine channel with the curvature of 4.0 mm. (a) 48 μL/min (0.01 m/s), (b) 144 μL/min (0.03 m/s), (c) 240 μL/min (0.05 m/s), (d) 336 μL/min (0.07 m/s), (e) 432 μL/min (0.09 m/s), (f) 528 μL/min (0.11 m/s), (g) 624 μL/min (0.13 m/s), (h) 720 μL/min (0.15 m/s), (i) 816 μL/min (0.17 m/s), (j) 912 μL/min (0.19 m/s), (k) 1008 μL/min (0.21 m/s), (l) 1104 μL/min (0.23 m/s), (m) 1296 μL/min (0.27 m/s), (n) 1488 μL/min (0.31 m/s), (o) 1680 μL/min (0.35 m/s), (p) 1872 μL/min (0.39 m/s), (q) 2064 μL/min (0.43 m/s), (r) 2256 μL/min (0.47 m/s), (s) 2448 μL/min (0.51 m/s), (t) 2640 μL/min (0.55 m/s), (u) 2832 μL/min (0.59 m/s).

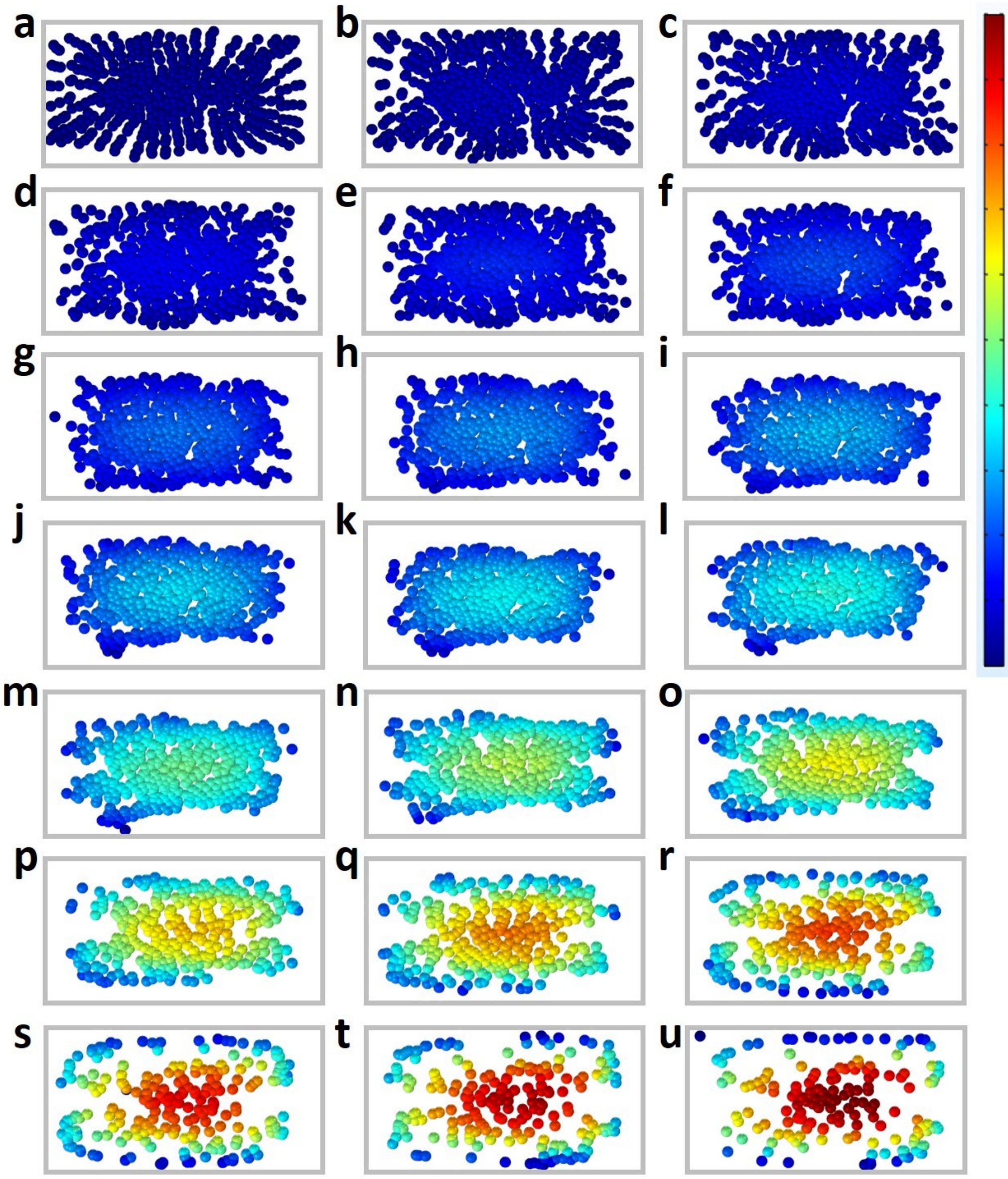

Fig. S3. The simulation results of different velocities (48 μL/min – 2832 μL/min) in serpentine channel with the curvature of 4.5 mm. (a) 48 μL/min (0.01 m/s), (b) 144 μL/min (0.03 m/s), (c) 240 μL/min (0.05 m/s), (d) 336 μL/min (0.07 m/s), (e) 432 μL/min (0.09 m/s), (f) 528 μL/min (0.11 m/s), (g) 624 μL/min (0.13 m/s), (h) 720 μL/min (0.15 m/s), (i) 816 μL/min (0.17 m/s), (j) 912 μL/min (0.19 m/s), (k) 1008 μL/min (0.21 m/s), (l) 1104 μL/min (0.23 m/s), (m) 1296 μL/min (0.27 m/s), (n) 1488 μL/min (0.31 m/s), (o) 1680 μL/min (0.35 m/s), (p) 1872 μL/min (0.39 m/s), (q) 2064 μL/min (0.43 m/s), (r) 2256 μL/min (0.47 m/s), (s) 2448 μL/min (0.51 m/s), (t) 2640 μL/min (0.55 m/s), (u) 2832 μL/min (0.59 m/s).

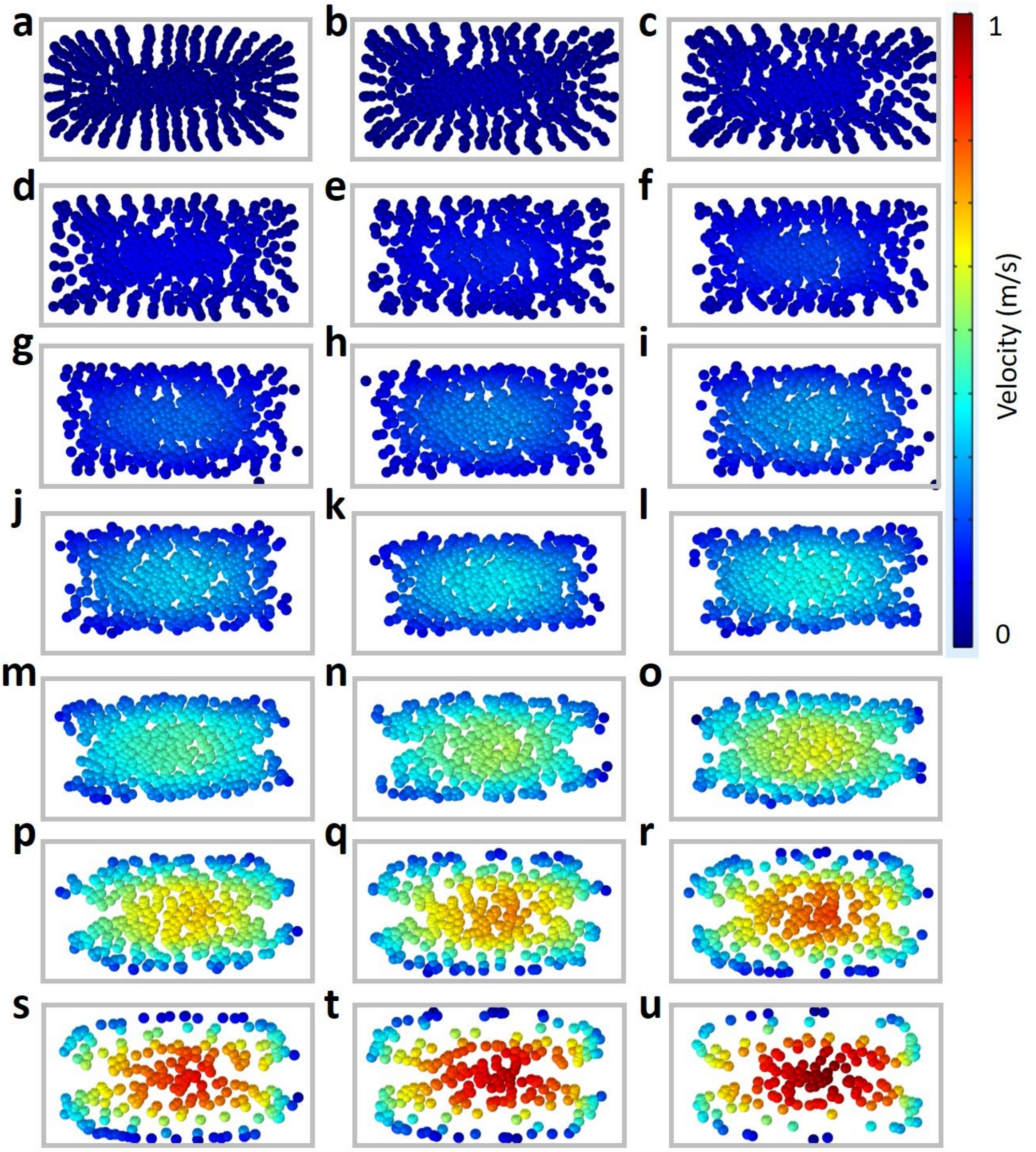

Fig. S4. The simulation results of different velocities (48 μL/min – 2832 μL/min) in serpentine channel with the curvature of 5.0 mm. (a) 48 μL/min (0.01 m/s), (b) 144 μL/min (0.03 m/s), (c) 240 μL/min (0.05 m/s), (d) 336 μL/min (0.07 m/s), (e) 432 μL/min (0.09 m/s), (f) 528 μL/min (0.11 m/s), (g) 624 μL/min (0.13 m/s), (h) 720 μL/min (0.15 m/s), (i) 816 μL/min (0.17 m/s), (j) 912 μL/min (0.19 m/s), (k) 1008 μL/min (0.21 m/s), (l) 1104 μL/min (0.23 m/s), (m) 1296 μL/min (0.27 m/s), (n) 1488 μL/min (0.31 m/s), (o) 1680 μL/min (0.35 m/s), (p) 1872 μL/min (0.39 m/s), (q) 2064 μL/min (0.43 m/s), (r) 2256 μL/min (0.47 m/s), (s) 2448 μL/min (0.51 m/s), (t) 2640 μL/min (0.55 m/s), (u) 2832 μL/min (0.59 m/s).

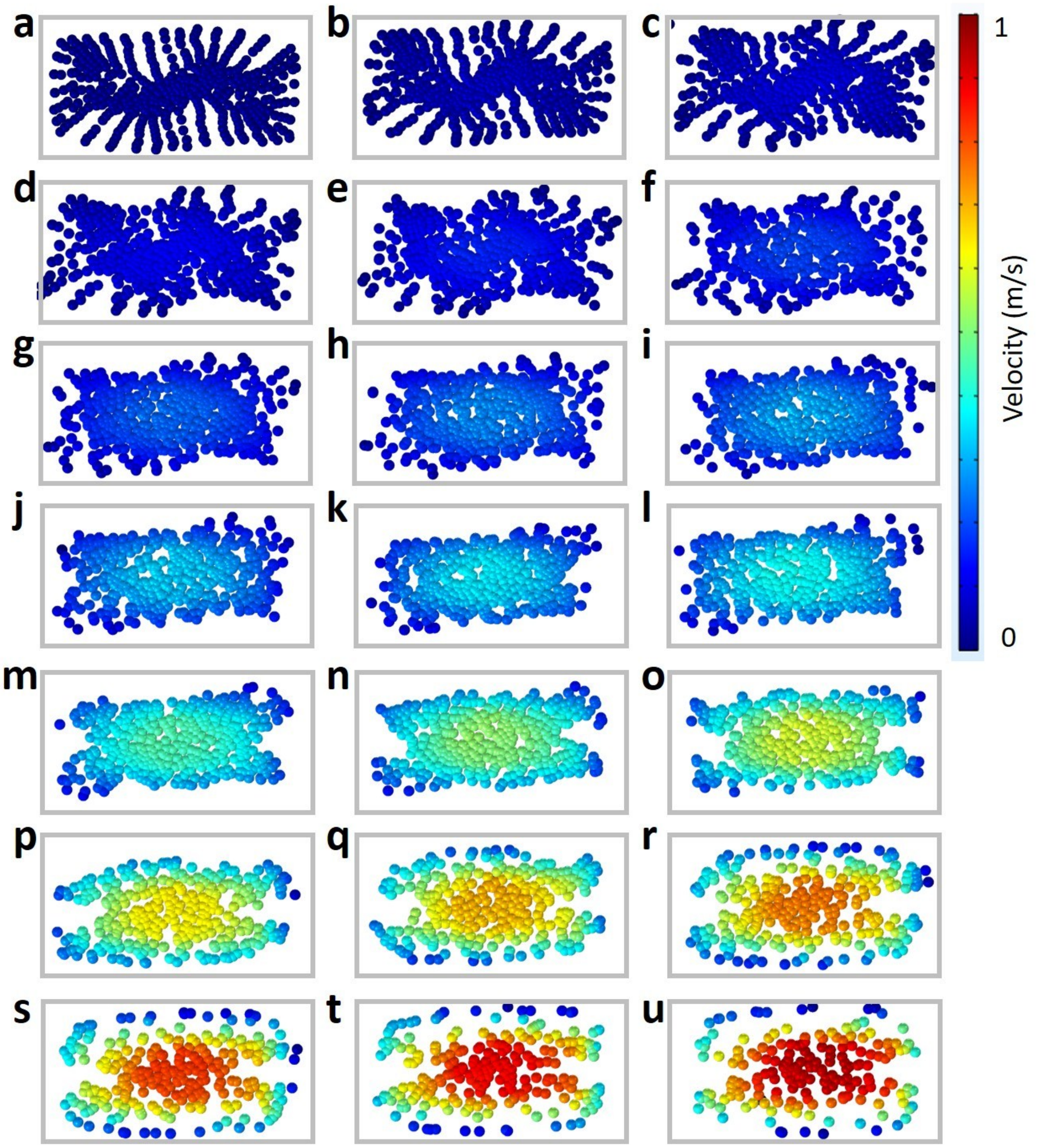

Fig. S5. The simulation results of different velocities (48 μL/min – 2832 μL/min) in serpentine channel with the curvature of 5.5 mm. (a) 48 μL/min (0.01 m/s), (b) 144 μL/min (0.03 m/s), (c) 240 μL/min (0.05 m/s), (d) 336 μL/min (0.07 m/s), (e) 432 μL/min (0.09 m/s), (f) 528 μL/min (0.11 m/s), (g) 624 μL/min (0.13 m/s), (h) 720 μL/min (0.15 m/s), (i) 816 μL/min (0.17 m/s), (j) 912 μL/min (0.19 m/s), (k) 1008 μL/min (0.21 m/s), (l) 1104 μL/min (0.23 m/s), (m) 1296 μL/min (0.27 m/s), (n) 1488 μL/min (0.31 m/s), (o) 1680 μL/min (0.35 m/s), (p) 1872 μL/min (0.39 m/s), (q) 2064 μL/min (0.43 m/s), (r) 2256 μL/min (0.47 m/s), (s) 2448 μL/min (0.51 m/s), (t) 2640 μL/min (0.55 m/s), (u) 2832 μL/min (0.59 m/s).

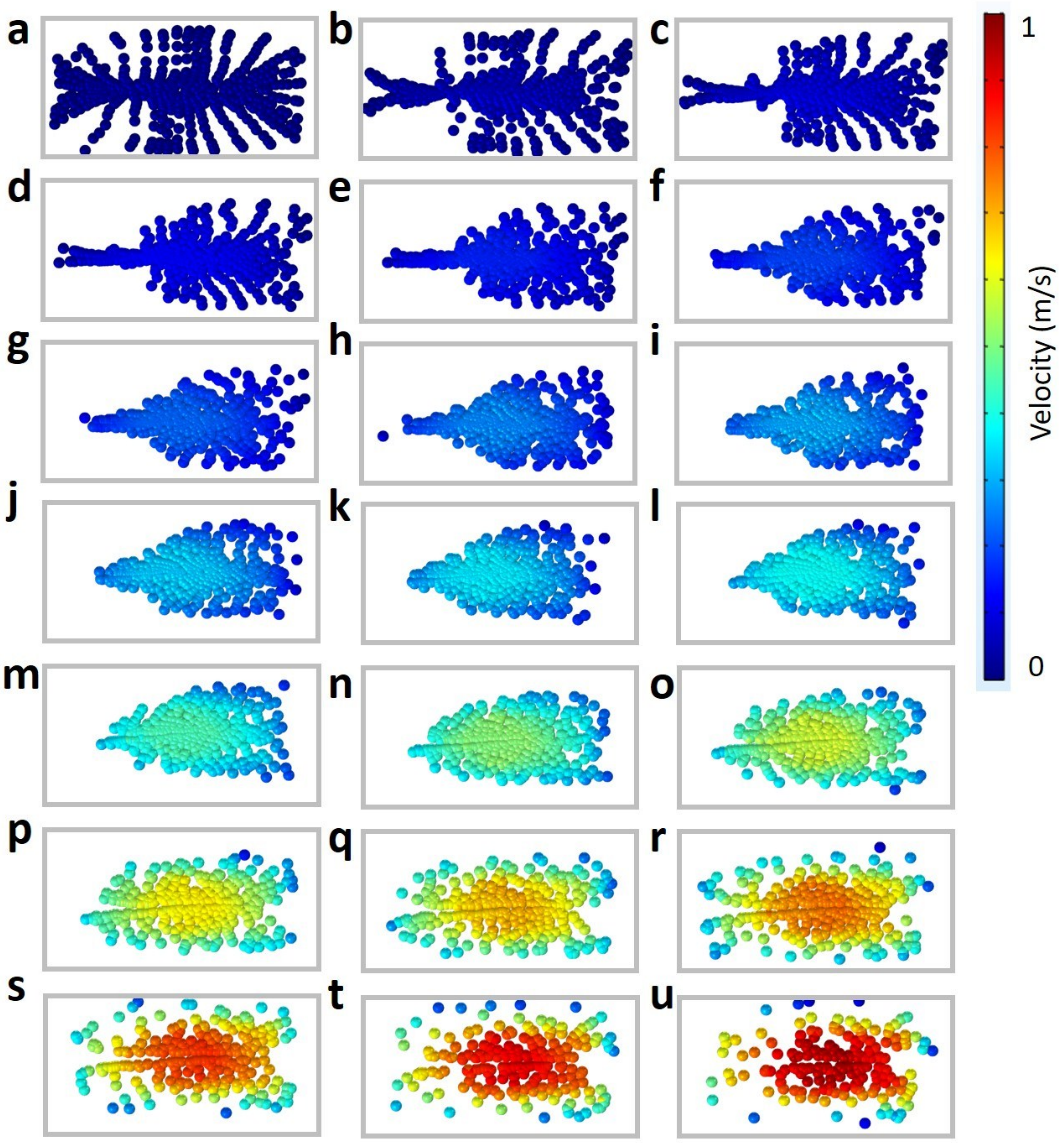

Fig. S6. The simulation results of different velocities (48 μL/min – 2832 μL/min) in serpentine channel with the curvature of 5.6 mm. (a) 48 μL/min (0.01 m/s), (b) 144 μL/min (0.03 m/s), (c) 240 μL/min (0.05 m/s), (d) 336 μL/min (0.07 m/s), (e) 432 μL/min (0.09 m/s), (f) 528 μL/min (0.11 m/s), (g) 624 μL/min (0.13 m/s), (h) 720 μL/min (0.15 m/s), (i) 816 μL/min (0.17 m/s), (j) 912 μL/min (0.19 m/s), (k) 1008 μL/min (0.21 m/s), (l) 1104 μL/min (0.23 m/s), (m) 1296 μL/min (0.27 m/s), (n) 1488 μL/min (0.31 m/s), (o) 1680 μL/min (0.35 m/s), (p) 1872 μL/min (0.39 m/s), (q) 2064 μL/min (0.43 m/s), (r) 2256 μL/min (0.47 m/s), (s) 2448 μL/min (0.51 m/s), (t) 2640 μL/min (0.55 m/s), (u) 2832 μL/min (0.59 m/s).

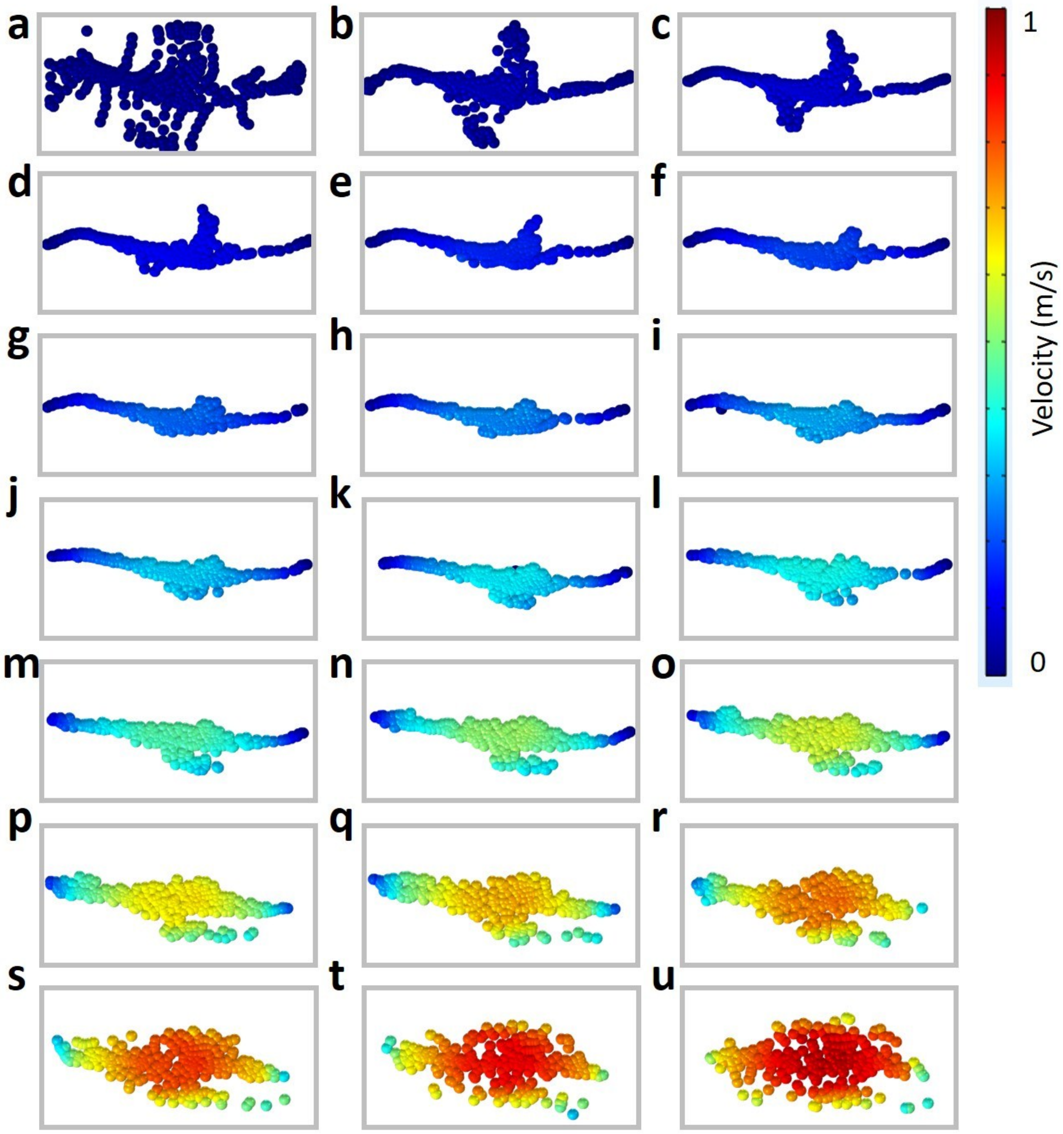

Fig. S7. The simulation results of different velocities (48 μL/min – 2832 μL/min) in serpentine channel with the curvature of 5.8 mm. (a) 48 μL/min (0.01 m/s), (b) 144 μL/min (0.03 m/s), (c) 240 μL/min (0.05 m/s), (d) 336 μL/min (0.07 m/s), (e) 432 μL/min (0.09 m/s), (f) 528 μL/min (0.11 m/s), (g) 624 μL/min (0.13 m/s), (h) 720 μL/min (0.15 m/s), (i) 816 μL/min (0.17 m/s), (j) 912 μL/min (0.19 m/s), (k) 1008 μL/min (0.21 m/s), (l) 1104 μL/min (0.23 m/s), (m) 1296 μL/min (0.27 m/s), (n) 1488 μL/min (0.31 m/s), (o) 1680 μL/min (0.35 m/s), (p) 1872 μL/min (0.39 m/s), (q) 2064 μL/min (0.43 m/s), (r) 2256 μL/min (0.47 m/s), (s) 2448 μL/min (0.51 m/s), (t) 2640 μL/min (0.55 m/s), (u) 2832 μL/min (0.59 m/s).

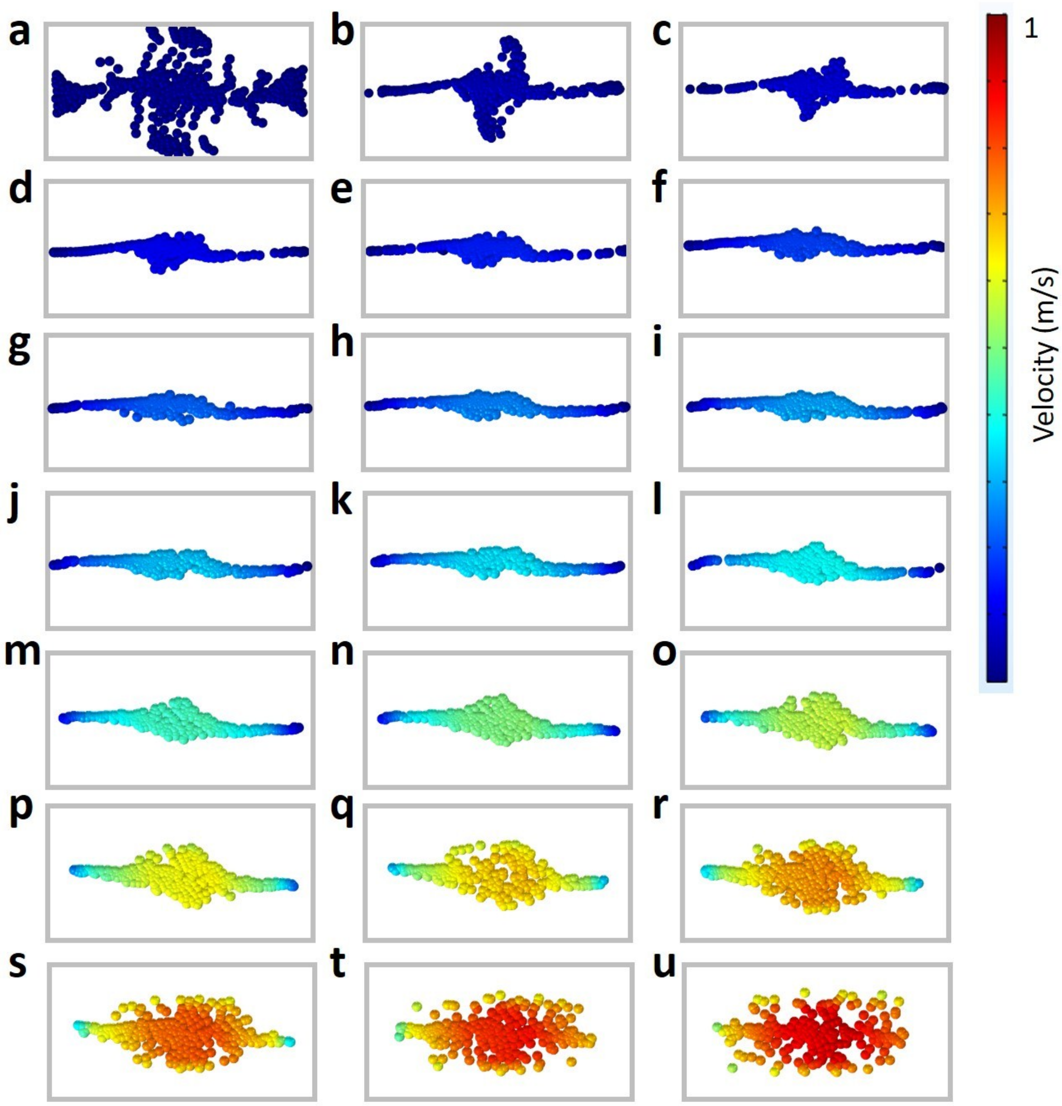

Fig. S8. The simulation results of different velocities (48 μL/min – 2832 μL/min) in serpentine channel with the curvature of 5.9 mm. (a) 48 μL/min (0.01 m/s), (b) 144 μL/min (0.03 m/s), (c) 240 μL/min (0.05 m/s), (d) 336 μL/min (0.07 m/s), (e) 432 μL/min (0.09 m/s), (f) 528 μL/min (0.11 m/s), (g) 624 μL/min (0.13 m/s), (h) 720 μL/min (0.15 m/s), (i) 816 μL/min (0.17 m/s), (j) 912 μL/min (0.19 m/s), (k) 1008 μL/min (0.21 m/s), (l) 1104 μL/min (0.23 m/s), (m) 1296 μL/min (0.27 m/s), (n) 1488 μL/min (0.31 m/s), (o) 1680 μL/min (0.35 m/s), (p) 1872 μL/min (0.39 m/s), (q) 2064 μL/min (0.43 m/s), (r) 2256 μL/min (0.47 m/s), (s) 2448 μL/min (0.51 m/s), (t) 2640 μL/min (0.55 m/s), (u) 2832 μL/min (0.59 m/s).

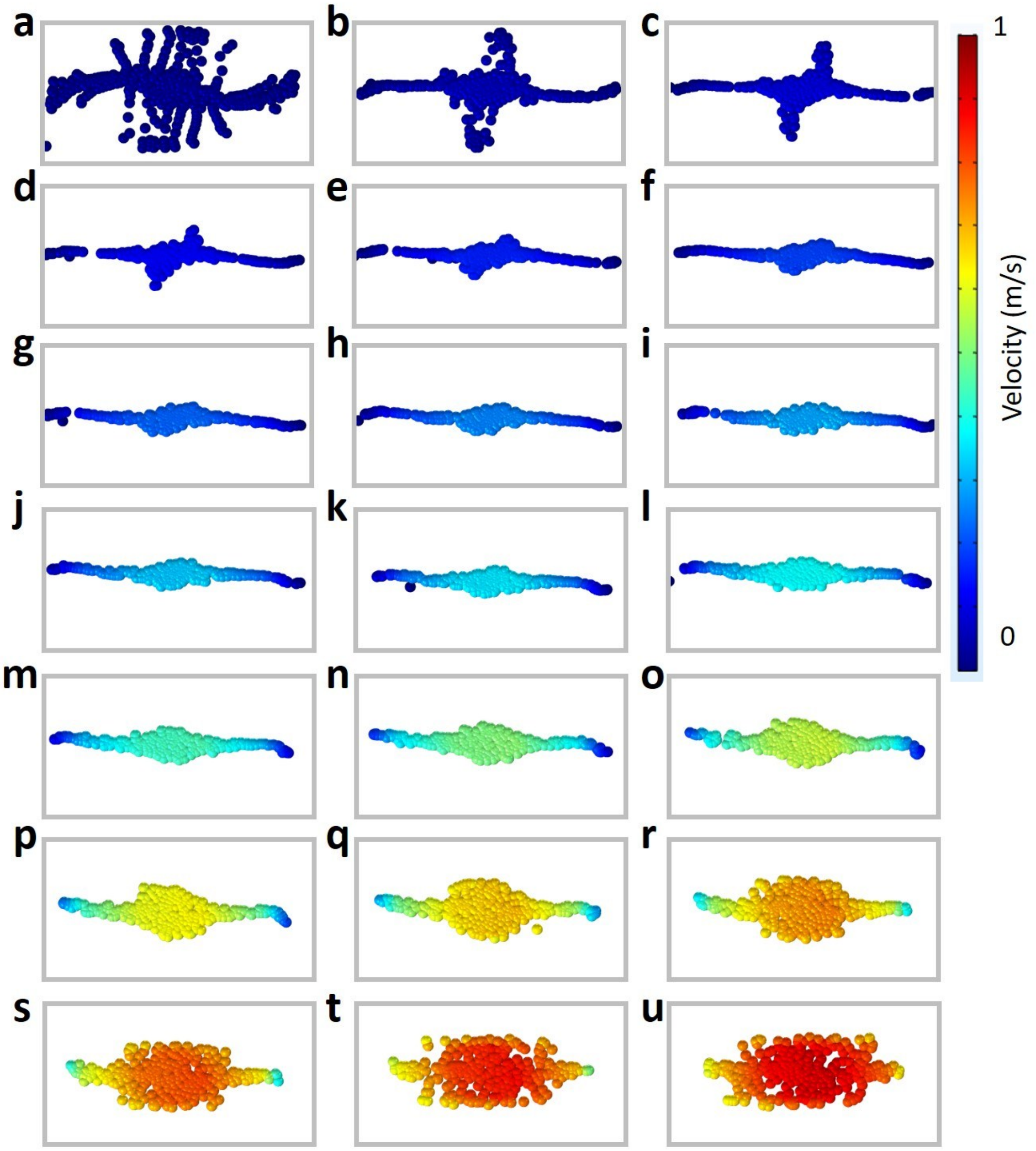

Fig. S9. The simulation results of different velocities (48 μL/min – 2832 μL/min) in serpentine channel with the curvature of 6.0 mm. (a) 48 μL/min (0.01 m/s), (b) 144 μL/min (0.03 m/s), (c) 240 μL/min (0.05 m/s), (d) 336 μL/min (0.07 m/s), (e) 432 μL/min (0.09 m/s), (f) 528 μL/min (0.11 m/s), (g) 624 μL/min (0.13 m/s), (h) 720 μL/min (0.15 m/s), (i) 816 μL/min (0.17 m/s), (j) 912 μL/min (0.19 m/s), (k) 1008 μL/min (0.21 m/s), (l) 1104 μL/min (0.23 m/s), (m) 1296 μL/min (0.27 m/s), (n) 1488 μL/min (0.31 m/s), (o) 1680 μL/min (0.35 m/s), (p) 1872 μL/min (0.39 m/s), (q) 2064 μL/min (0.43 m/s), (r) 2256 μL/min (0.47 m/s), (s) 2448 μL/min (0.51 m/s), (t) 2640 μL/min (0.55 m/s), (u) 2832 μL/min (0.59 m/s).

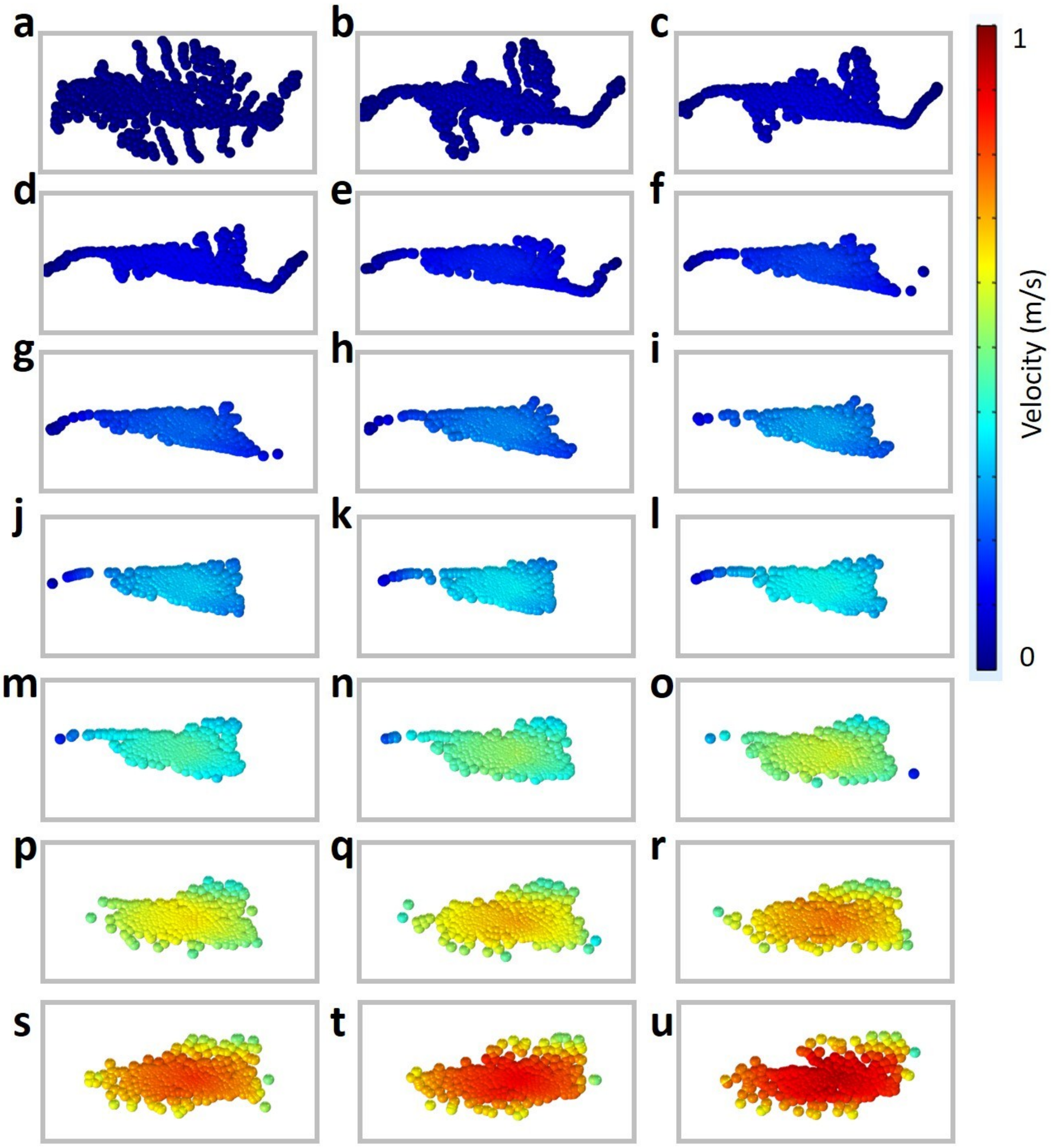

Fig. S10. The simulation results of different velocities (48 μL/min – 2832 μL/min) in serpentine channel with the curvature of 6.2 mm. (a) 48 μL/min (0.01 m/s), (b) 144 μL/min (0.03 m/s), (c) 240 μL/min (0.05 m/s), (d) 336 μL/min (0.07 m/s), (e) 432 μL/min (0.09 m/s), (f) 528 μL/min (0.11 m/s), (g) 624 μL/min (0.13 m/s), (h) 720 μL/min (0.15 m/s), (i) 816 μL/min (0.17 m/s), (j) 912 μL/min (0.19 m/s), (k) 1008 μL/min (0.21 m/s), (l) 1104 μL/min (0.23 m/s), (m) 1296 μL/min (0.27 m/s), (n) 1488 μL/min (0.31 m/s), (o) 1680 μL/min (0.35 m/s), (p) 1872 μL/min (0.39 m/s), (q) 2064 μL/min (0.43 m/s), (r) 2256 μL/min (0.47 m/s), (s) 2448 μL/min (0.51 m/s), (t) 2640 μL/min (0.55 m/s), (u) 2832 μL/min (0.59 m/s).

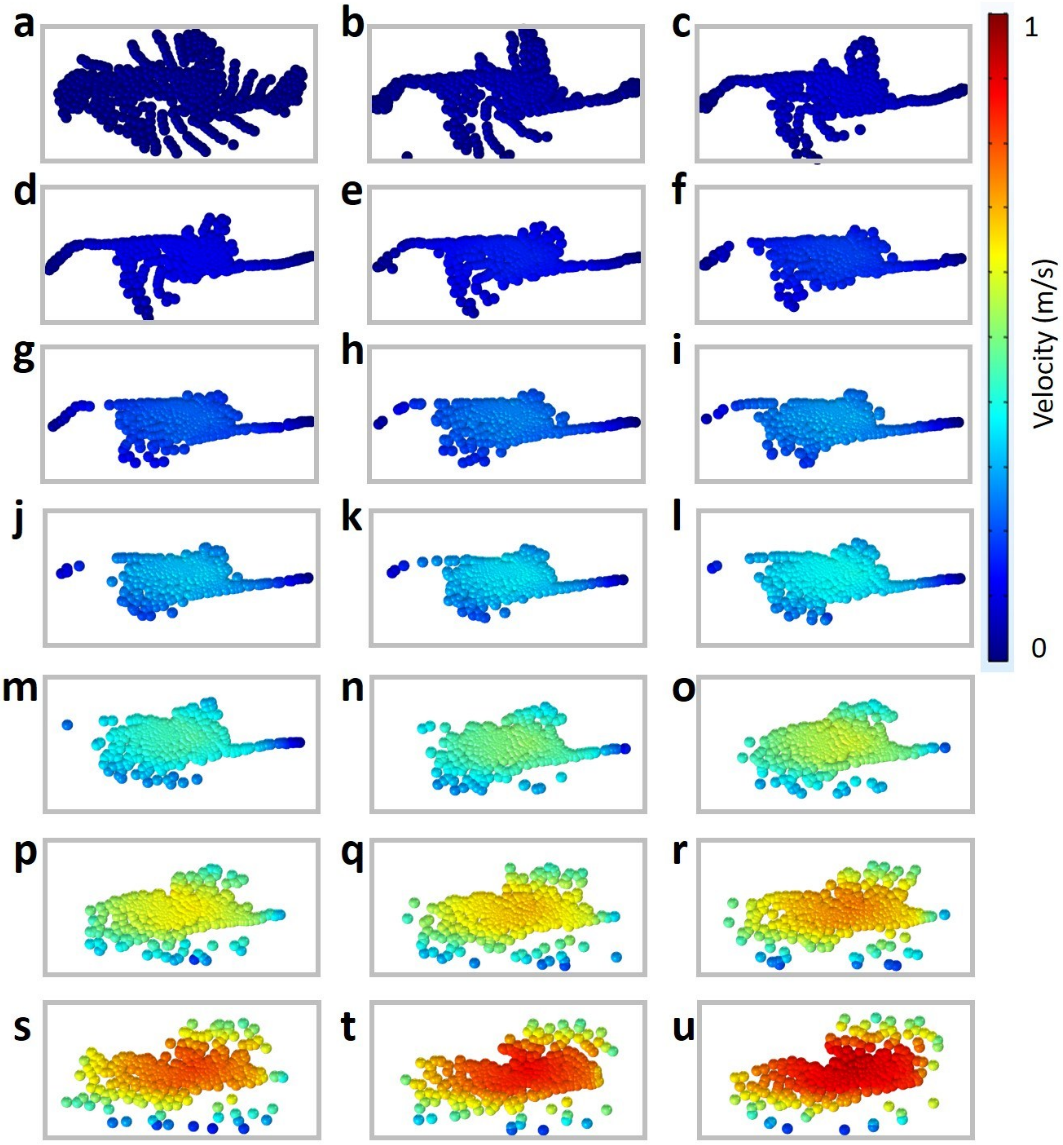

Fig. S11. The simulation results of different velocities (48 µL/min – 2832 µL/min) in serpentine channel with the curvature of 6.4 mm. (a) 48 µL/min (0.01 m/s), (b) 144 µL/min (0.03 m/s), (c) 240 µL/min (0.05 m/s), (d) 336 µL/min (0.07 m/s), (e) 432 µL/min (0.09 m/s), (f) 528 µL/min (0.11 m/s), (g) 624 µL/min (0.13 m/s), (h) 720 µL/min (0.15 m/s), (i) 816 µL/min (0.17 m/s), (j) 912 µL/min (0.19 m/s), (k) 1008 µL/min (0.21 m/s), (l) 1104 µL/min (0.23 m/s), (m) 1296 µL/min (0.27 m/s), (n) 1488 µL/min (0.31 m/s), (o) 1680 µL/min (0.35 m/s), (p) 1872 µL/min (0.39 m/s), (q) 2064 µL/min (0.43 m/s), (r) 2256 µL/min (0.47 m/s), (s) 2448 µL/min (0.51 m/s), (t) 2640 µL/min (0.55 m/s), (u) 2832 µL/min (0.59 m/s).

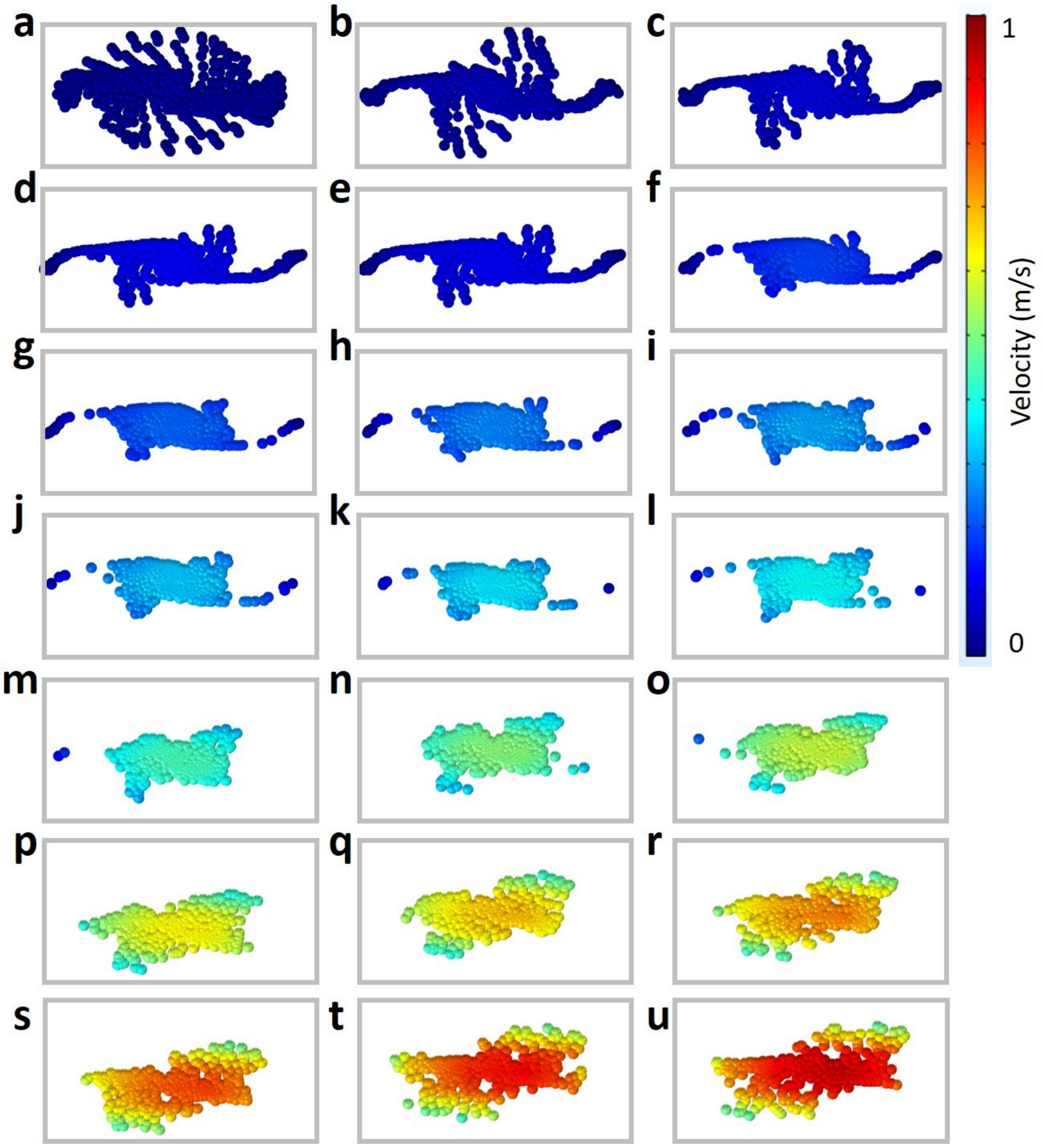

Fig. S12. The simulation results of different velocities (48 μL/min – 2832 μL/min) in serpentine channel with the curvature of 6.5 mm. (a) 48 μL/min (0.01 m/s), (b) 144 μL/min (0.03 m/s), (c) 240 μL/min (0.05 m/s), (d) 336 μL/min (0.07 m/s), (e) 432 μL/min (0.09 m/s), (f) 528 μL/min (0.11 m/s), (g) 624 μL/min (0.13 m/s), (h) 720 μL/min (0.15 m/s), (i) 816 μL/min (0.17 m/s), (j) 912 μL/min (0.19 m/s), (k) 1008 μL/min (0.21 m/s), (l) 1104 μL/min (0.23 m/s), (m) 1296 μL/min (0.27 m/s), (n) 1488 μL/min (0.31 m/s), (o) 1680 μL/min (0.35 m/s), (p) 1872 μL/min (0.39 m/s), (q) 2064 μL/min (0.43 m/s), (r) 2256 μL/min (0.47 m/s), (s) 2448 μL/min (0.51 m/s), (t) 2640 μL/min (0.55 m/s), (u) 2832 μL/min (0.59 m/s).

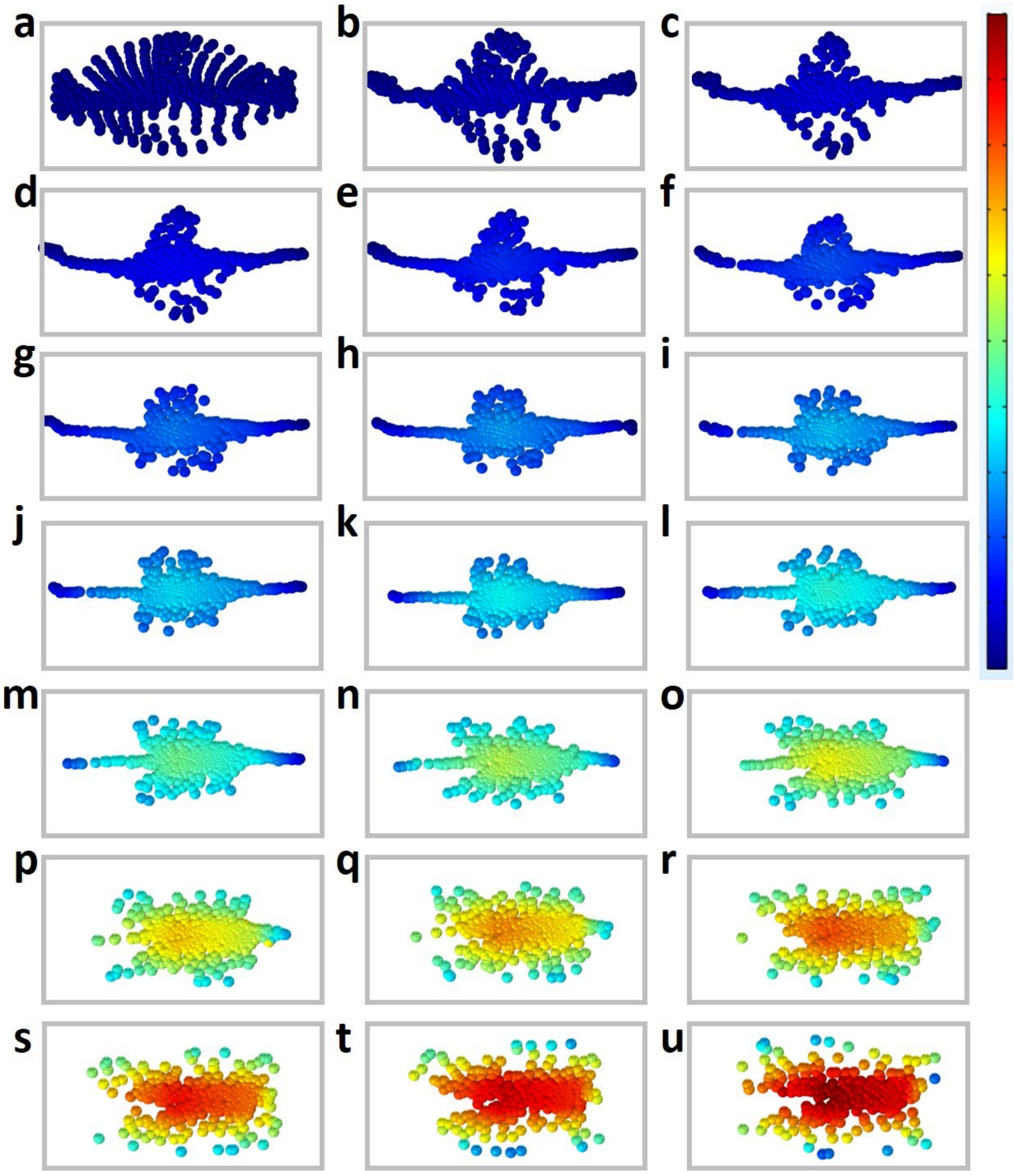

Fig. S13. The simulation results of different velocities (48 μL/min – 2832 μL/min) in serpentine channel with the curvature of 6.6 mm. (a) 48 μL/min (0.01 m/s), (b) 144 μL/min (0.03 m/s), (c) 240 μL/min (0.05 m/s), (d) 336 μL/min (0.07 m/s), (e) 432 μL/min (0.09 m/s), (f) 528 μL/min (0.11 m/s), (g) 624 μL/min (0.13 m/s), (h) 720 μL/min (0.15 m/s), (i) 816 μL/min (0.17 m/s), (j) 912 μL/min (0.19 m/s), (k) 1008 μL/min (0.21 m/s), (l) 1104 μL/min (0.23 m/s), (m) 1296 μL/min (0.27 m/s), (n) 1488 μL/min (0.31 m/s), (o) 1680 μL/min (0.35 m/s), (p) 1872 μL/min (0.39 m/s), (q) 2064 μL/min (0.43 m/s), (r) 2256 μL/min (0.47 m/s), (s) 2448 μL/min (0.51 m/s), (t) 2640 μL/min (0.55 m/s), (u) 2832 μL/min (0.59 m/s).

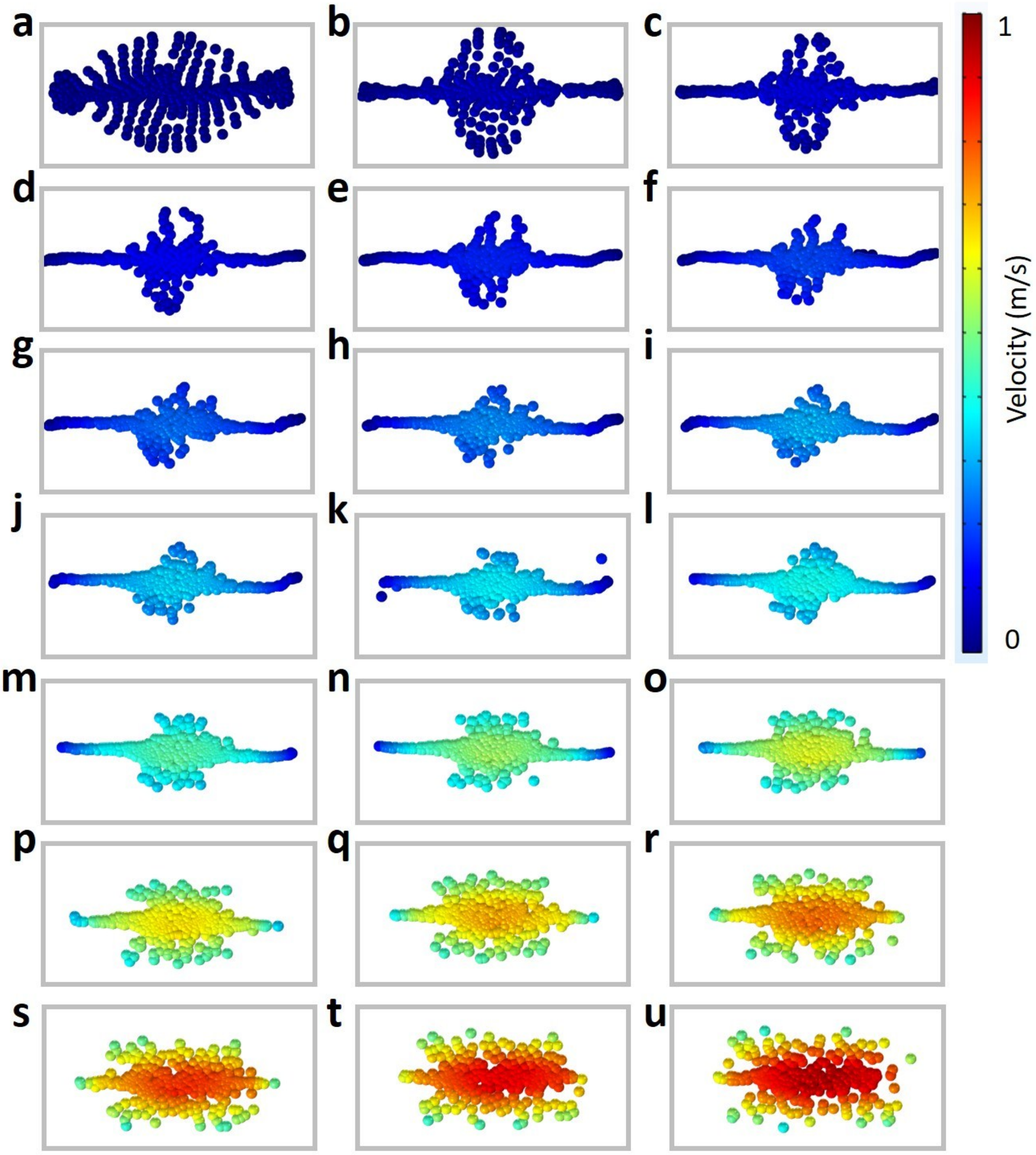

Fig. S14. The simulation results of different velocities (48 μL/min – 2832 μL/min) in serpentine channel with the curvature of 7.0 mm. (a) 48 μL/min (0.01 m/s), (b) 144 μL/min (0.03 m/s), (c) 240 μL/min (0.05 m/s), (d) 336 μL/min (0.07 m/s), (e) 432 μL/min (0.09 m/s), (f) 528 μL/min (0.11 m/s), (g) 624 μL/min (0.13 m/s), (h) 720 μL/min (0.15 m/s), (i) 816 μL/min (0.17 m/s), (j) 912 μL/min (0.19 m/s), (k) 1008 μL/min (0.21 m/s), (l) 1104 μL/min (0.23 m/s), (m) 1296 μL/min (0.27 m/s), (n) 1488 μL/min (0.31 m/s), (o) 1680 μL/min (0.35 m/s), (p) 1872 μL/min (0.39 m/s), (q) 2064 μL/min (0.43 m/s), (r) 2256 μL/min (0.47 m/s), (s) 2448 μL/min (0.51 m/s), (t) 2640 μL/min (0.55 m/s), (u) 2832 μL/min (0.59 m/s).

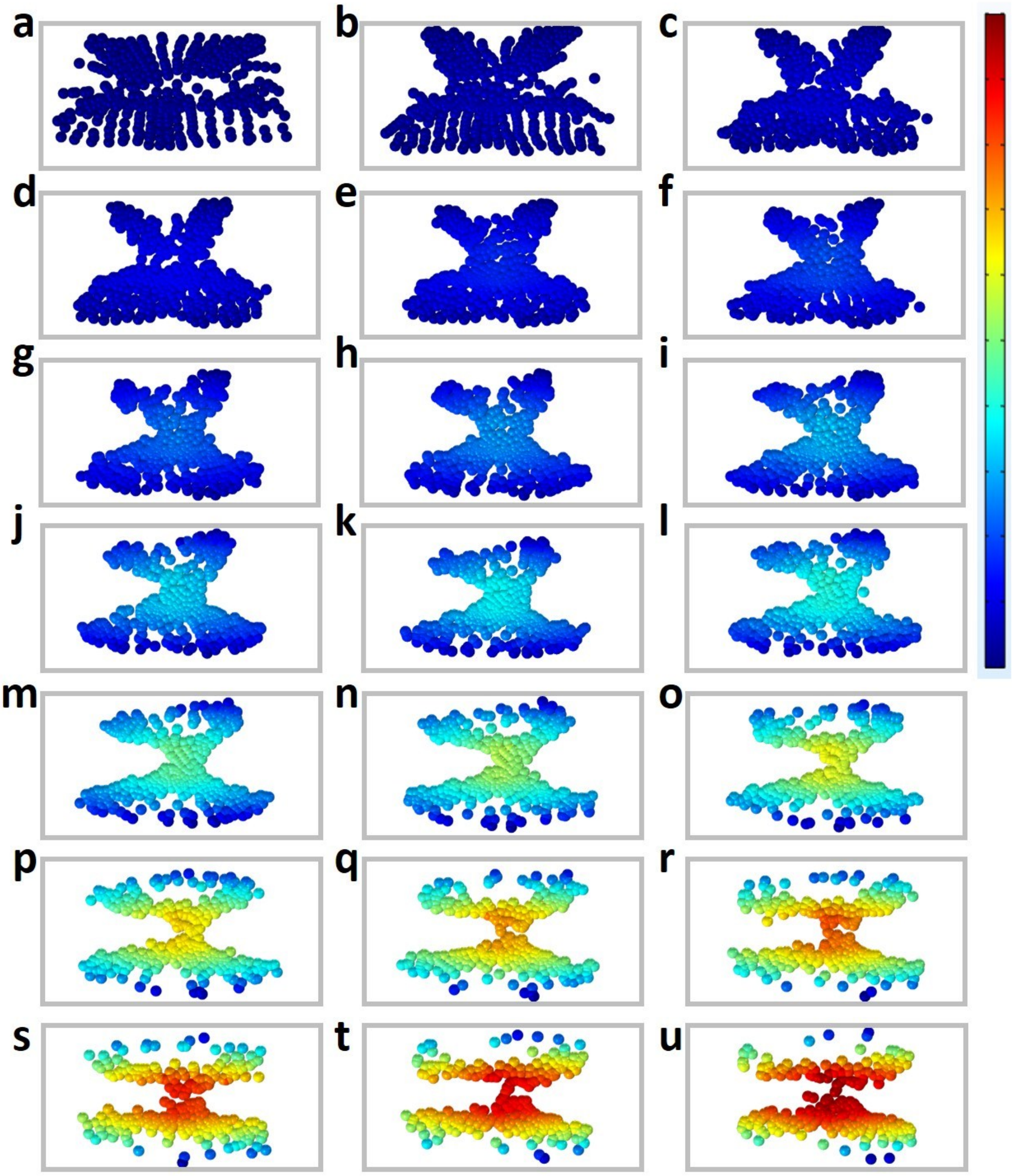

Fig. S15. The simulation results of different velocities (48 μL/min – 2832 μL/min) in serpentine channel with the curvature of 7.5 mm. (a) 48 μL/min (0.01 m/s), (b) 144 μL/min (0.03 m/s), (c) 240 μL/min (0.05 m/s), (d) 336 μL/min (0.07 m/s), (e) 432 μL/min (0.09 m/s), (f) 528 μL/min (0.11 m/s), (g) 624 μL/min (0.13 m/s), (h) 720 μL/min (0.15 m/s), (i) 816 μL/min (0.17 m/s), (j) 912 μL/min (0.19 m/s), (k) 1008 μL/min (0.21 m/s), (l) 1104 μL/min (0.23 m/s), (m) 1296 μL/min (0.27 m/s), (n) 1488 μL/min (0.31 m/s), (o) 1680 μL/min (0.35 m/s), (p) 1872 μL/min (0.39 m/s), (q) 2064 μL/min (0.43 m/s), (r) 2256 μL/min (0.47 m/s), (s) 2448 μL/min (0.51 m/s), (t) 2640 μL/min (0.55 m/s), (u) 2832 μL/min (0.59 m/s).

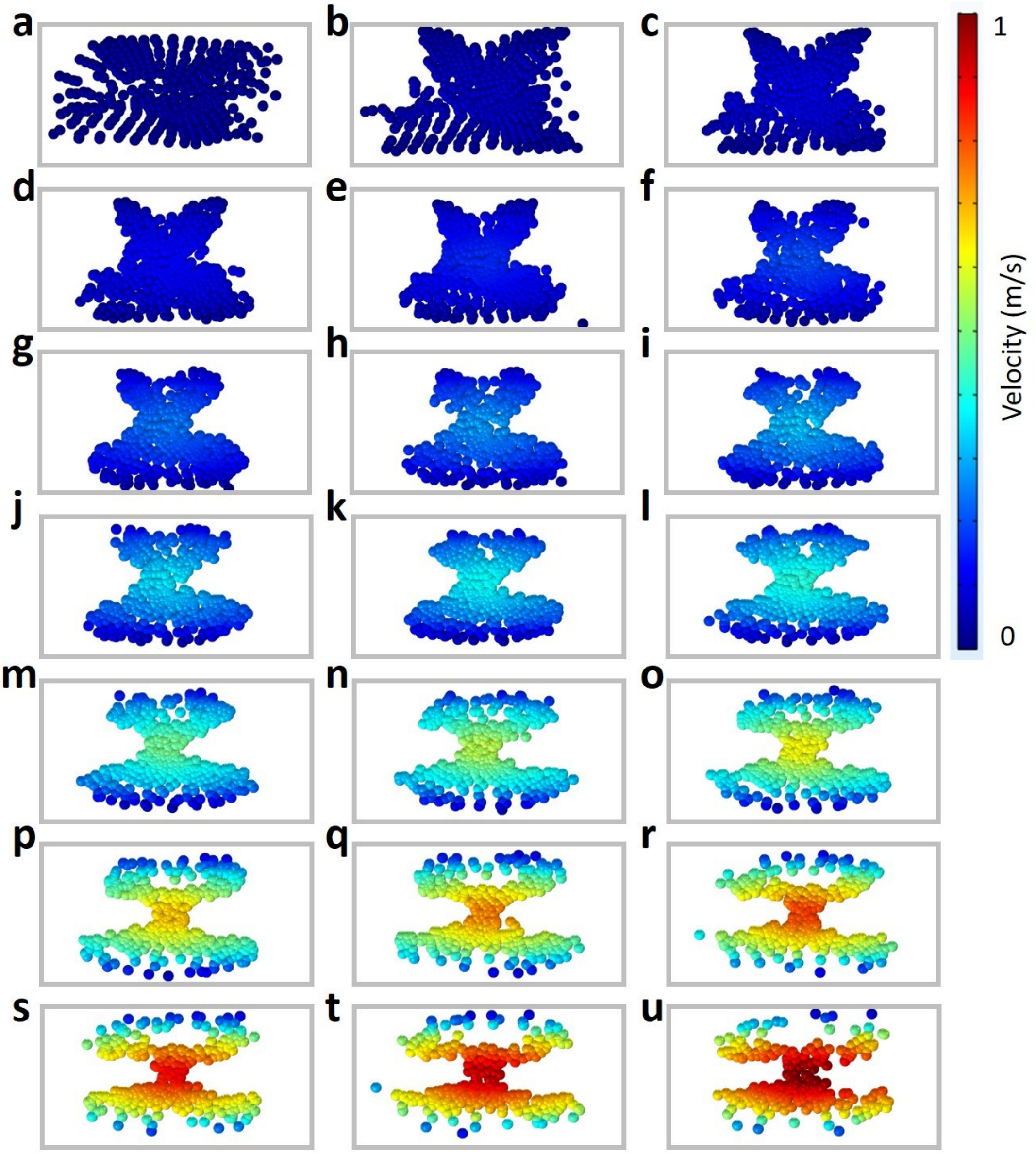

Fig. S16. The simulation results of different velocities (48 μL/min – 2832 μL/min) in serpentine channel with the curvature of 8.0 mm. (a) 48 μL/min (0.01 m/s), (b) 144 μL/min (0.03 m/s), (c) 240 μL/min (0.05 m/s), (d) 336 μL/min (0.07 m/s), (e) 432 μL/min (0.09 m/s), (f) 528 μL/min (0.11 m/s), (g) 624 μL/min (0.13 m/s), (h) 720 μL/min (0.15 m/s), (i) 816 μL/min (0.17 m/s), (j) 912 μL/min (0.19 m/s), (k) 1008 μL/min (0.21 m/s), (l) 1104 μL/min (0.23 m/s), (m) 1296 μL/min (0.27 m/s), (n) 1488 μL/min (0.31 m/s), (o) 1680 μL/min (0.35 m/s), (p) 1872 μL/min (0.39 m/s), (q) 2064 μL/min (0.43 m/s), (r) 2256 μL/min (0.47 m/s), (s) 2448 μL/min (0.51 m/s), (t) 2640 μL/min (0.55 m/s), (u) 2832 μL/min (0.59 m/s).

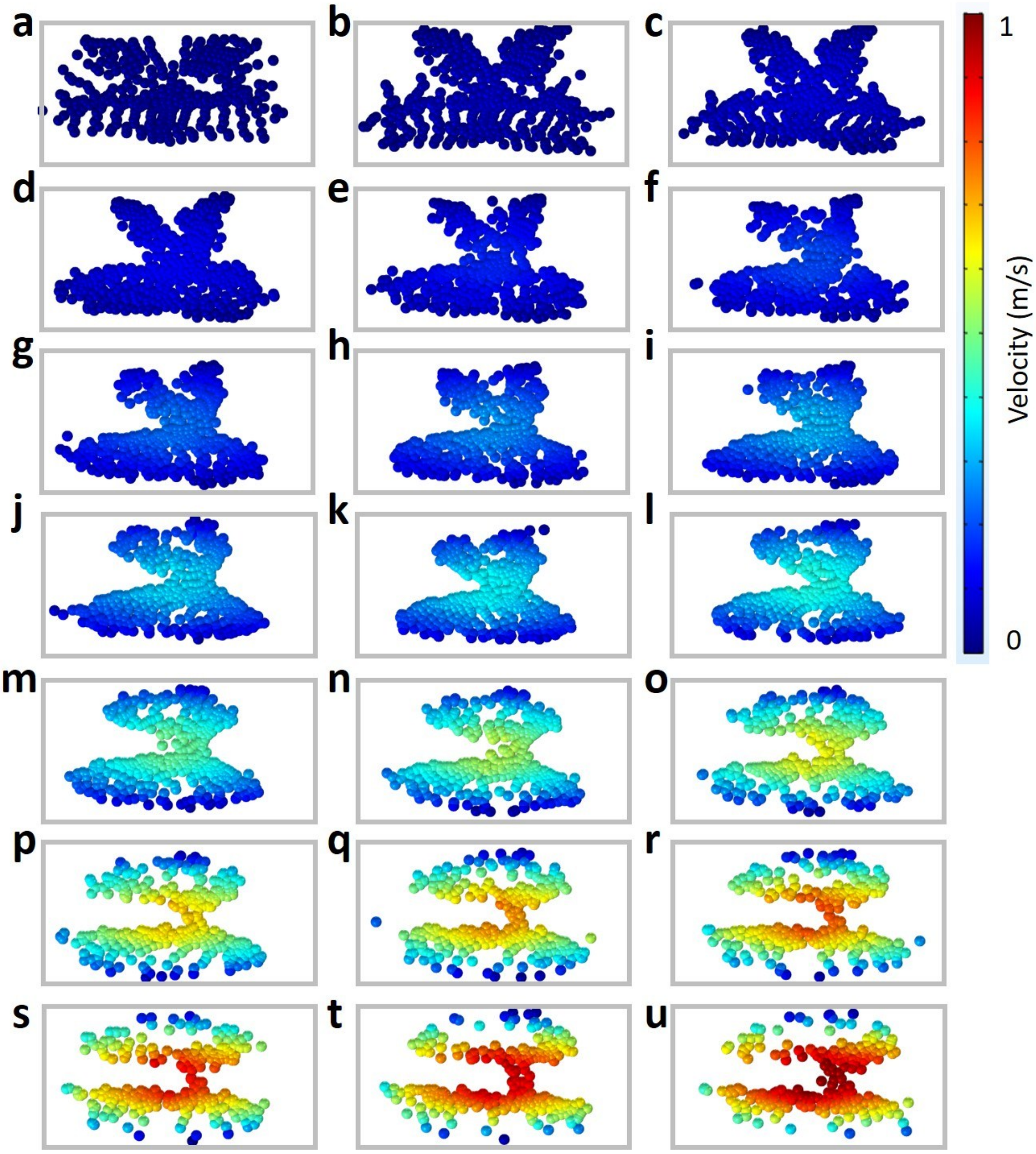

Fig. S17. The simulation results of different velocities (48 μL/min – 2832 μL/min) in serpentine channel with the curvature of 8.5 mm. (a) 48 μL/min (0.01 m/s), (b) 144 μL/min (0.03 m/s), (c) 240 μL/min (0.05 m/s), (d) 336 μL/min (0.07 m/s), (e) 432 μL/min (0.09 m/s), (f) 528 μL/min (0.11 m/s), (g) 624 μL/min (0.13 m/s), (h) 720 μL/min (0.15 m/s), (i) 816 μL/min (0.17 m/s), (j) 912 μL/min (0.19 m/s), (k) 1008 μL/min (0.21 m/s), (l) 1104 μL/min (0.23 m/s), (m) 1296 μL/min (0.27 m/s), (n) 1488 μL/min (0.31 m/s), (o) 1680 μL/min (0.35 m/s), (p) 1872 μL/min (0.39 m/s), (q) 2064 μL/min (0.43 m/s), (r) 2256 μL/min (0.47 m/s), (s) 2448 μL/min (0.51 m/s), (t) 2640 μL/min (0.55 m/s), (u) 2832 μL/min (0.59 m/s).

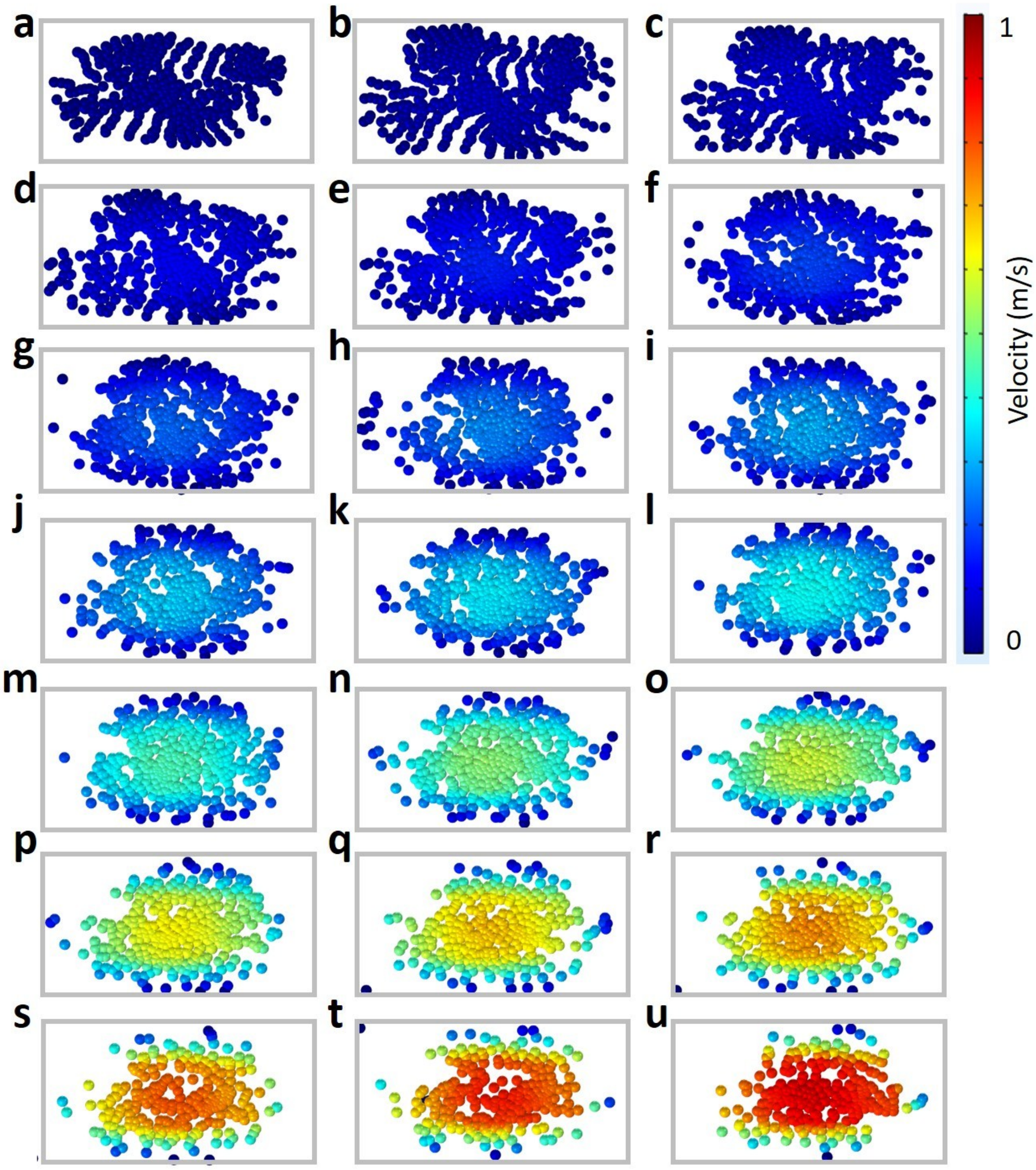

Fig. S18. The simulation results of different velocities (48 μL/min – 2832 μL/min) in serpentine channel with the curvature of 9.0 mm. (a) 48 μL/min (0.01 m/s), (b) 144 μL/min (0.03 m/s), (c) 240 μL/min (0.05 m/s), (d) 336 μL/min (0.07 m/s), (e) 432 μL/min (0.09 m/s), (f) 528 μL/min (0.11 m/s), (g) 624 μL/min (0.13 m/s), (h) 720 μL/min (0.15 m/s), (i) 816 μL/min (0.17 m/s), (j) 912 μL/min (0.19 m/s), (k) 1008 μL/min (0.21 m/s), (l) 1104 μL/min (0.23 m/s), (m) 1296 μL/min (0.27 m/s), (n) 1488 μL/min (0.31 m/s), (o) 1680 μL/min (0.35 m/s), (p) 1872 μL/min (0.39 m/s), (q) 2064 μL/min (0.43 m/s), (r) 2256 μL/min (0.47 m/s), (s) 2448 μL/min (0.51 m/s), (t) 2640 μL/min (0.55 m/s), (u) 2832 μL/min (0.59 m/s).

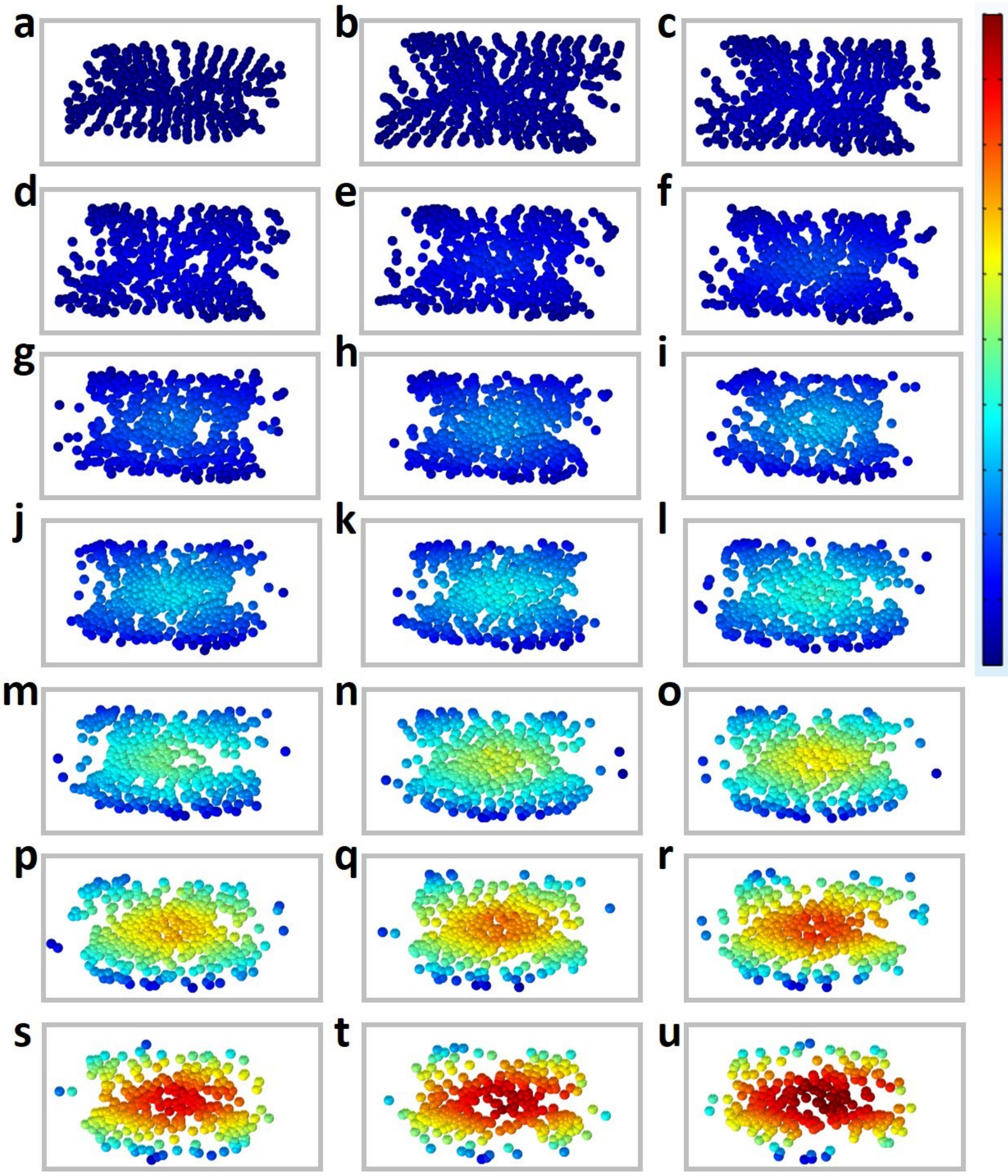

Fig. S19. The simulation results of different velocities (48 μL/min – 2832 μL/min) in serpentine channel with the curvature of 10.0 mm. (a) 48 μL/min (0.01 m/s), (b) 144 μL/min (0.03 m/s), (c) 240 μL/min (0.05 m/s), (d) 336 μL/min (0.07 m/s), (e) 432 μL/min (0.09 m/s), (f) 528 μL/min (0.11 m/s), (g) 624 μL/min (0.13 m/s), (h) 720 μL/min (0.15 m/s), (i) 816 μL/min (0.17 m/s), (j) 912 μL/min (0.19 m/s), (k) 1008 μL/min (0.21 m/s), (l) 1104 μL/min (0.23 m/s), (m) 1296 μL/min (0.27 m/s), (n) 1488 μL/min (0.31 m/s), (o) 1680 μL/min (0.35 m/s), (p) 1872 μL/min (0.39 m/s), (q) 2064 μL/min (0.43 m/s), (r) 2256 μL/min (0.47 m/s), (s) 2448 μL/min (0.51 m/s), (t) 2640 μL/min (0.55 m/s), (u) 2832 μL/min (0.59 m/s).

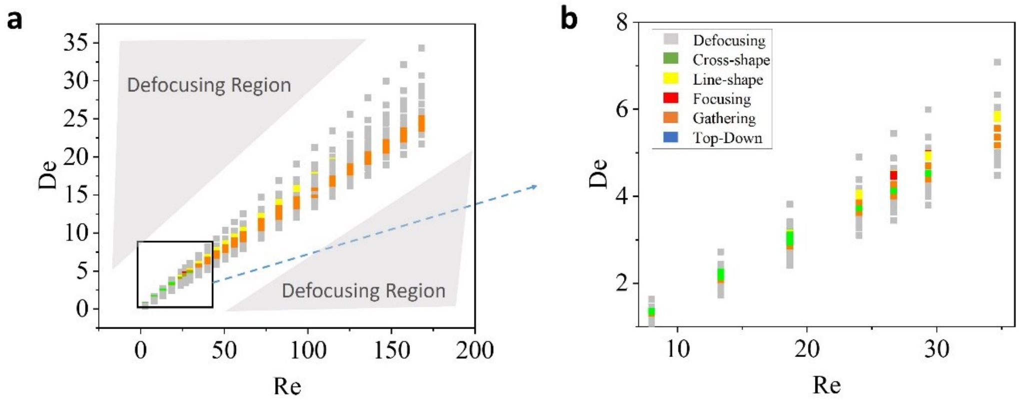

Fig. S20. Summarize the simulation results to six focusing status by dimensionless numbers (Re-De). (a) All simulation data in Fig. 4. The legend of (a) is the same as (b). (b) Partial enlarged detail in (a).

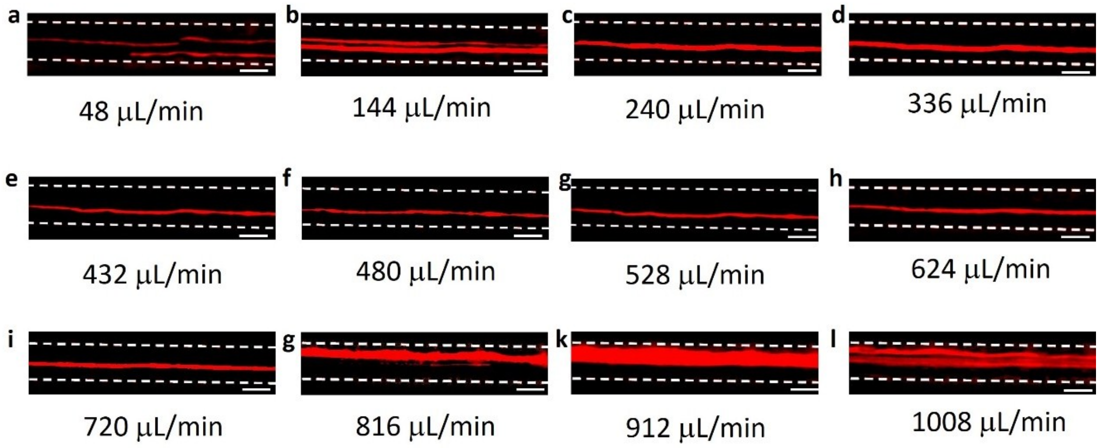

Fig. S21. Experimental results at the outlet of the microfluidic channels with 5.9 mm curvature radius by different flow throughput. Scale bar 200 μm.

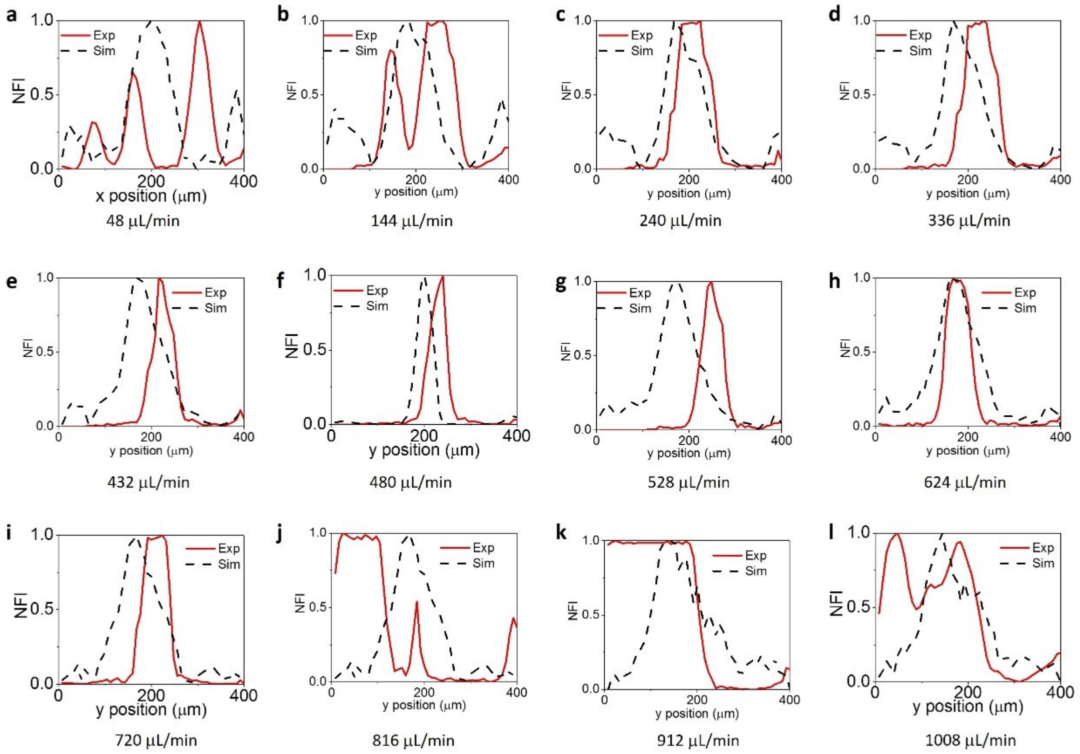

Fig. S22. the statistics of simulated and experiment data by NFI In the different fluid flow throughput (48 μL/min – 1008 μL/min) with 5.9 mm curvature radius.

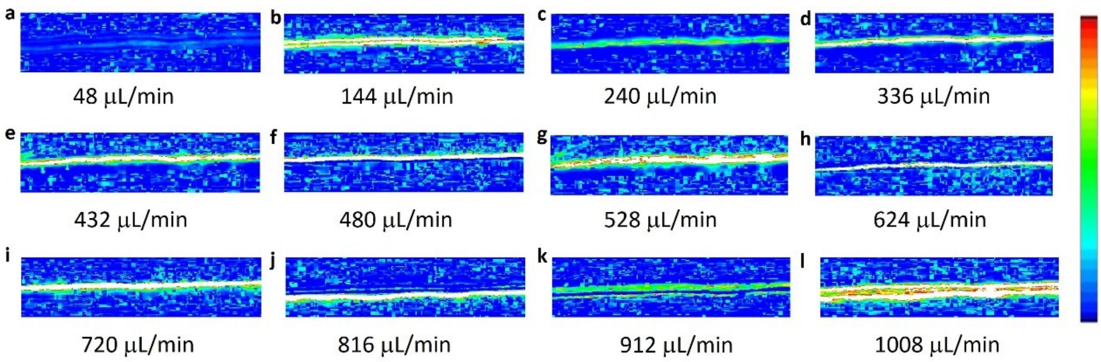

Fig. S23. The heat maps of experiments data in different fluid flow throughput (48 μL/min – 1008 μL/min) with 5.9 mm curvature radius.

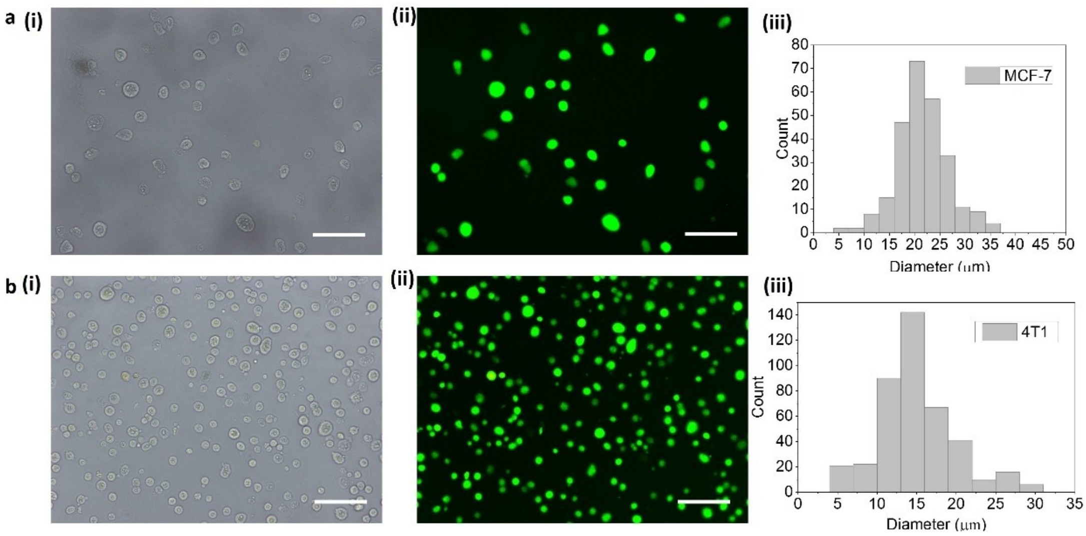

Fig. S24. Images and sizes of MCF-7 and 4T1 cancer cells. (a) Bright images (i), fluorescent images (ii) and the size distribution of MCF-7 cancer cells. (b) Bright images (i), fluorescent images (ii) and the size distribution of 4T1 cancer cells.

Table S2. The dimensionless number (Re, De) in different channel radius (2mm-5.85mm) and flow velocity (0.01m/s-0.59m/s).

r(mm) / Vel(m/s)	2mm	3mm	4mm	4.5mm	5mm	5.5mm	5.8mm	5.85mm
0.01	2.98,0.77	2.98,0.63	2.98,0.54	2.98,0.51	2.98,0.49	2.98,0.46	2.98,0.45	2.98,0.45
0.03	8.95,2.31	8.95,1.89	8.95,1.63	8.95,1.54	8.95,1.46	8.95,1.39	8.95,1.36	8.95,1.35
0.05	14.92,3.85	14.92,3.15	14.92,2.72	14.92,2.57	14.92,2.44	14.92,2.32	14.92,2.26	14.92,2.25
0.07	20.89,5.39	20.89,4.4	20.89,3.81	20.89,3.6	20.89,3.41	20.89,3.25	20.89,3.17	20.89,3.15
0.09	26.86,6.93	26.86,5.66	26.86,4.9	26.86,4.62	26.86,4.39	26.86,4.18	26.86,4.07	26.86,4.05
0.1	29.84,7.71	29.84,6.29	29.84,5.45	29.84,5.14	29.84,4.87	29.84,4.65	29.84,4.52	29.84,4.51
0.11	32.83,8.48	32.83,6.92	32.83,5.99	32.83,5.65	32.83,5.36	32.83,5.11	32.83,4.98	32.83,4.96
0.13	38.79,10.02	38.79,8.18	38.79,7.08	38.79,6.68	38.79,6.34	38.79,6.04	38.79,5.88	38.79,5.86
0.15	44.76,11.56	44.76,9.44	44.76,8.17	44.76,7.71	44.76,7.31	44.76,6.97	44.76,6.79	44.76,6.76
0.17	50.73,13.1	50.73,10.7	50.73,9.26	50.73,8.73	50.73,8.28	50.73,7.9	50.73,7.69	50.73,7.66
0.19	56.7,14.64	56.7,11.95	56.7,10.35	56.7,9.76	56.7,9.26	56.7,8.83	56.7,8.6	56.7,8.56
0.21	62.67,16.18	62.67,13.21	62.67,11.44	62.67,10.79	62.67,10.23	62.67,9.76	62.67,9.5	62.67,9.46
0.23	68.64,17.72	68.64,14.47	68.64,12.53	68.64,11.81	68.64,11.21	68.64,10.69	68.64,10.41	68.64,10.36
0.27	80.57,20.8	80.57,16.99	80.57,14.71	80.57,13.87	80.57,13.16	80.57,12.55	80.57,12.22	80.57,12.16
0.31	92.51,23.89	92.51,19.5	92.51,16.89	92.51,15.92	92.51,15.11	92.51,14.4	92.51,14.03	92.51,13.97
0.35	104.45,26.97	104.45,22.02	104.45,19.07	104.45,17.98	104.45,17.06	104.45,16.26	104.45,15.84	104.45,15.77
0.39	116.38,30.05	116.38,24.54	116.38,21.25	116.38,20.03	116.38,19.01	116.38,18.12	116.38,17.65	116.38,17.57
0.43	128.32,33.13	128.32,27.05	128.32,23.43	128.32,22.09	128.32,20.95	128.32,19.98	128.32,19.46	128.32,19.37
0.47	140.26,36.21	140.26,29.57	140.26,25.61	140.26,24.14	140.26,22.9	140.26,21.84	140.26,21.27	140.26,21.17
0.51	152.19,39.3	152.19,32.09	152.19,27.79	152.19,26.2	152.19,24.85	152.19,23.7	152.19,23.08	152.19,22.98
0.55	164.13,42.38	164.13,34.6	164.13,29.97	164.13,28.25	164.13,26.8	164.13,25.56	164.13,24.89	164.13,24.78
0.59	176.07,45.46	176.07,37.12	176.07,32.15	176.07,30.31	176.07,28.75	176.07,27.41	176.07,26.7	176.07,26.58

Table S3. The dimensionless number (Re, De) in different channel radius (5.9mm-10mm) and flow velocity (0.01m/s-0.59m/s).

r(mm) / Vel(m/s)	5.9mm	5.95mm	6mm	6.5mm	7mm	8mm	9mm	10mm
0.01	2.98,0.45	2.98,0.45	2.98,0.44	2.98,0.43	2.98,0.41	2.98,0.39	2.98,0.36	2.98,0.34
0.03	8.95,1.35	8.95,1.34	8.95,1.33	8.95,1.28	8.95,1.24	8.95,1.16	8.95,1.09	8.95,1.03
0.05	14.92,2.24	14.92,2.23	14.92,2.22	14.92,2.14	14.92,2.06	14.92,1.93	14.92,1.82	14.92,1.72
0.07	20.89,3.14	20.89,3.13	20.89,3.11	20.89,2.99	20.89,2.88	20.89,2.7	20.89,2.54	20.89,2.41
0.09	26.86,4.04	26.86,4.02	26.86,4	26.86,3.85	26.86,3.71	26.86,3.47	26.86,3.27	26.86,3.1
0.1	29.84,4.49	29.84,4.47	29.84,4.45	29.84,4.27	29.84,4.12	29.84,3.85	29.84,3.63	29.84,3.45
0.11	32.83,4.93	32.83,4.91	32.83,4.89	32.83,4.7	32.83,4.53	32.83,4.24	32.83,4	32.83,3.79
0.13	38.79,5.83	38.79,5.81	38.79,5.78	38.79,5.56	38.79,5.35	38.79,5.01	38.79,4.72	38.79,4.48
0.15	44.76,6.73	44.76,6.7	44.76,6.67	44.76,6.41	44.76,6.18	44.76,5.78	44.76,5.45	44.76,5.17
0.17	50.73,7.63	50.73,7.59	50.73,7.56	50.73,7.27	50.73,7	50.73,6.55	50.73,6.17	50.73,5.86
0.19	56.7,8.52	56.7,8.49	56.7,8.45	56.7,8.12	56.7,7.83	56.7,7.32	56.7,6.9	56.7,6.55
0.21	62.67,9.42	62.67,9.38	62.67,9.34	62.67,8.98	62.67,8.65	62.67,8.09	62.67,7.63	62.67,7.24
0.23	68.64,10.32	68.64,10.27	68.64,10.23	68.64,9.83	68.64,9.47	68.64,8.86	68.64,8.35	68.64,7.93
0.27	80.57,12.11	80.57,12.06	80.57,12.01	80.57,11.54	80.57,11.12	80.57,10.4	80.57,9.81	80.57,9.3
0.31	92.51,13.91	92.51,13.85	92.51,13.79	92.51,13.25	92.51,12.77	92.51,11.94	92.51,11.26	92.51,10.68
0.35	104.45,15.7	104.45,15.64	104.45,15.57	104.45,14.96	104.45,14.42	104.45,13.48	104.45,12.71	104.45,12.06
0.39	116.38,17.5	116.38,17.42	116.38,17.35	116.38,16.67	116.38,16.06	116.38,15.03	116.38,14.17	116.38,13.44
0.43	128.32,19.29	128.32,19.21	128.32,19.13	128.32,18.38	128.32,17.71	128.32,16.57	128.32,15.62	128.32,14.82
0.47	140.26,21.08	140.26,21	140.26,20.91	140.26,20.09	140.26,19.36	140.26,18.11	140.26,17.07	140.26,16.2
0.51	152.19,22.88	152.19,22.78	152.19,22.69	152.19,21.8	152.19,21	152.19,19.65	152.19,18.52	152.19,17.57
0.55	164.13,24.67	164.13,24.57	164.13,24.47	164.13,23.51	164.13,22.65	164.13,21.19	164.13,19.98	164.13,18.95
0.59	176.07,26.47	176.07,26.36	176.07,26.25	176.07,25.22	176.07,24.3	176.07,22.73	176.07,21.43	176.07,20.33